Journal of Materials Chemistry A

Accepted Manuscript

ROYAL SOCIETY OF CHEMISTRY

www.rsc.org/materialsA

Journal Name

RSCPublishing

Article

A crosslinked fullerene matrix doped with an ionic fullerene as a cathodic buffer layer toward high-performance and thermally stable polymer and organic metallohalide perovskite solar cells

Cite this: DOI: 10.1039/xoxxoooooox

Received ooth January 2012,
Accepted ooth January 2012

DOI: 10.1039/xoxxoooooox

www.rsc.org/

Yi-Hsiang Chao,[a] Yi-You Huang, [a] Jen-Yun Chang,[a] Shih-Hao Peng, [a] Wei-Yi Tu, [a] Yen-Ju Cheng, [a] Jianhui Hou, [b] and Chain-Shu Hsu.* [a]

In this study, we developed a new cathodic buffer layer consisting of a cross-linked [6,6]-phenyl-C_{61}-butyric styryl dendron ester (C-PCBSD) matrix and an ionic FPI dopant. The incorporation of FPI can improve the electron mobility via an anion induced charge transfer (AIET) mechanism while maintaining the solvent-resistant property of the crosslinked layer. The ZnO combined with C-PCBSD/FPI layer can effectively and universally improve the performance of bulk-heterojunction polymer solar cells (BHJPSCs), planar heterojunction polymer solar cells (PHJPSCs), and organic metallohalide perovskite solar cells (OMPSCs). Furthermore, the insertion of C-PCBSD/FPI layer can improve the thermal stability of the device by preventing the residue moisture in ZnO from diffusing into the $CH_3NH_3PbI_3$ layer in OMPSCs.

1. Introduction

Organic metallohalide perovskite solar cells (OMPSCs) have swiftly emerged as the most promising solution to the energy issue due to the significant progress in the power conversion efficiencies (PCEs) over 10%.[1-14] In 2009, Miyasaka and coworkers first utilized $CH_3NH_3PbI_3$ as a visible-light sensitizer with mesoporous TiO_2 as the cathodic buffer layer (CBL) to obtain a PCE of 3.9%.[15] Later on, Park and coworkers optimized the thickness of mesoporous TiO_2 layer with a post-annealing treatment on the perovskite thin film to achieve a PCE of 6.5%.[16] On the other hand, Snaith and coworkers used 2,2′,7,7′-tetrakis(*N*,*N*-di-p-methoxyphenylamine)-9,9-spirobifluorene (spiro-OMeTAD) as a hole-collecting layer to achieve a high PCE of 10%.[17] Very recently, Yang and coworkers further improved the performance up to 19% via interfacial layer modifications.[18]

Along with the performances, the practical uses of OMPSCs reply on the device stability as well as the fabrication cost.[19-22] TiO_2 has been widely used as the cathodic buffer layer to achieve high-performance $CH_3NH_3PbI_3$-based perovskite solar cells. However, the TiO_2-coated OMPSCs usually require high-temperature sintering processes that hinder roll-to-roll production.[23] Furthermore, TiO_2 decrease the device's stability due to the UV-induced degradation.[24] On the other hand, ZnO is another promising CBL candidate for OMPSCs as a result of its good electron mobility.[25] However, high sensitivity of ZnO to humidity in nature is also detrimental to the $CH_3NH_3PbI_3$.[26] To overcome the humidity issue, deposition of a functional fullerene layer on ZnO to enhance the air-stability might be a good strategy for OMPSCs.[27] We recently reported a crosslinked [6,6]-phenyl-C61-butyric styryl dendron ester (C-PCBSD) interlayer showing hole-blocking ability and facilitating electron transfer in the inverted PSCs.[28-30] It is envisaged that the C-PCBSD layer can generate a smoother and more hydrophobic surface on ZnO to block moisture and thus improve the device lifetime. Nevertheless, the intrinsic low mobility of C-PCBSD interlayer may constraint the charge collection and transport between active layer and electrode.[31-34] Recently, Jen and coworkers incorporated an ionic fullerene dopant, bis-fulleropyrrolidium iodide (Bis-FPI), into a cross-linked fullerene matrix to facilitate electron transport and provide conductive pathway via an anion-induced charge transfer (AIET) mechanism leading to much enhanced performance.[35-37] Nevertheless, utilization of this method has never been reported in the OMPSCs. In this research, we wish to report a fullerene derivative FPI as shown in **Figure 1** which was doped into a solvent-resistant C-PCBSD layer for the fabrication of the inverted devices of BHJPSCs and OMPSCs.[38] The electron mobility of the 50 wt% FPI-doped C-PCBSD increases significantly by four times compared to the pure C-PCBSD layer. Because of extra exciton dissociation with reduced series resistance, the device with ITO/ZnO/FPI-doped C-PCBSD/$CH_3NH_3PbI_3$/Spiro-OMeTAD/Au exhibited an

impressive PCE of 11.9% with a V_{oc} of 0.90 V, a J_{sc} of 19.1 mA/cm^2, and an *FF* of 69%.

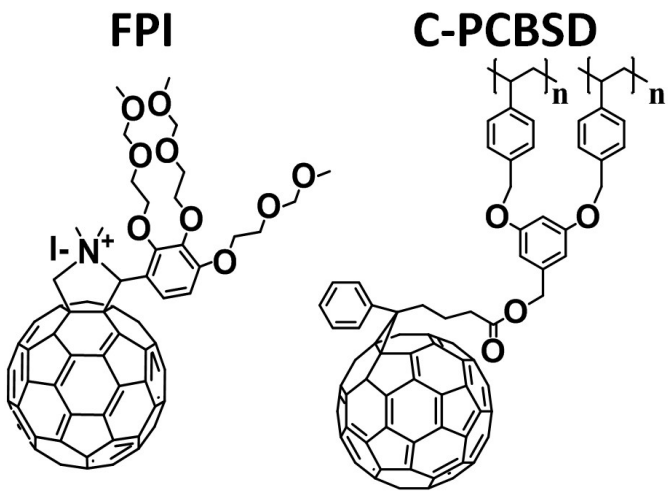

Figure 1. Chemical structures of FPI an C-PCBSD

2. Experimental Section

2.1 Device fabrication procedures

For the device fabrication of BHJPSCs and planar heterojunction polymer solar cells (PHJPSCs), ITO glass substrates (purchased from Wintek; sheet resistance 30 Ω sq−1) were cleaned with detergent, deionized water, acetone, and isopropyl alcohol (IPA) in an ultrasonic bath and then dried overnight in an oven at >100 ℃. Zinc acetate dihydrate (Sigma-Aldrich) dissolved in 2-metoxyenthanol (Sigma-Aldrich, 10 mg mL^{-1}) and small amount of ethanolamine (Sigma-Aldrich) was spin-casted on pre-cleaned ITO substrates and baked at 170 ℃ for 10 minutes in the air to form the ZnO layer with thickness of 40 nm.[39] PCBSD, PCBSD (FPI, 25%), and PCBSD (FPI,50%) were dissolved in ODCB to a concentration of 0.5 wt%. For devices fabricated with C-PCBSD or C-PCBSD with FPI dopant interlayer, the solution was spin-casted onto the ZnO layer to form a thin film with a thickness of ca. 10 nm. Subsequently, the film was annealed at 170 ℃ for 10 minutes in the glove box for thermal cross-linking. For Device fabricated with polymer, P3HT (Lumtec Corp.) were dissolved in ODCB (1.5 wt %), and PC61BM (Lumtec Corp.) was then added into the solution to reach the desired weight ratio. For Device fabricated with low band gap polymer, PBDTTT-C-T were dissolved in ODCB (0.77 wt %), and $PC_{71}BM$ was then added into the solution to reach the desired weight ratio if needed. The solution was stirred at 70 ^oC for overnight and filtrated through a 0.45 um filter. The activelayers were then spin-coated onto the ZnO layer with desired thickness, and the diiodooctane (DIO) was added 3 v% to the solution before spin-coating if using PBDTTT-C-T : $PC_{71}BM$ solution.[40] The anode made of MoO_3 (6 nm) and Ag(150 nm) was evaporated through a shadow mask under vacuum (<10^{-6} Torr).

The procedure of cleaning substrate, and CBL coating in OMPSCs are as the same as in BHJPSCs. The PbI_2 solution (Sigma-Aldrich) dissolving in *N*,*N*-dimethylformamide (DMF) at a concentration of 460 mg mL^{-1} was spin-coated on top of the ZnO layer at 3000 rpm 15s. After drying for 15 minutes in the glove box, the substrate was heated in hot plate for 70 ℃ for 10 minutes. Then, the substrate was dipped into the solution of CH_3NH_3I (FrontMaterials Co. Ltd) in anhydrous IPA (10 mg mL^{-1}) for 40s and washed by IPA. Subsequently, the solution of spiro-OMeTAD purchased from FrontMaterials Co. Ltd (80 mg spiro-OMeTAD, 28.5 ml 4-tertbutylpyridine and 17.5 ml lithium-bis(trifluoromethanesulfonyl)imide (Li-TFSI) (520 mg Li-TFSI in 1 ml acetonitrile) all dissolved in 1 ml chlorobenzene) was spin-coating at 4,000 rpm for 30 s. Finally, Au (80 nm) was evaporated through a shadow mask under vacuum (<10^{-6} Torr). Each sample consists of four independent pixels defined by an active area of 0.04 cm^2

2.2 Device characterization

The devices were encapsulated and characterized in air under 100 mW/cm^2 AM 1.5 simulated light measurement (Yamashita Denso solar simulator). Current−voltage (*J*−*V*) characteristics of the PSCs were obtained by a Keithley 2400 SMU. Solar illumination conforming the JIS Class AAA was provided by a SAN-EI 300W solar simulator equipped with an AM 1.5G filter. The light intensity was calibrated with a Hamamatsu S1336-5BK silicon photodiode. IPCE spectra were measured using a lock-in amplifier with a current preamplifier under short-circuit conditions with illumination by monochromatic light from a 250 W quartz-halogen lamp (Osram) passing through a monochromator (Spectral Products CM110).

2.3 Thin film characterization

Absorption spectra were acquired by HP 8453 spectrophotometer. For the measurement of electron mobility in BHJPSCs devices, the space charge limited current (SCLC) was adopted according literature. [41] For devices fabricated with C-PCBSD or C-PCBSD with FPI dopant interlayer, the solution was spin-casted onto the ZnO layer. Subsequently, the film was annealed at 170 ℃ for 15 minutes in the glove box for thermal cross-linking. The blend solutions containing P3HT/$PC_{61}BM$ (1:1, w/w) were spin-casted on top of the C-PCBSD layer. Finally, the top electrode, made of Ca (10 nm)/Al (100 nm), was thermally evaporated at a pressure below 10^{-6} torr to complete the devices. The electron mobility can be estimated by Mott-Gurney's equation, $J = (9\varepsilon\varepsilon_o\mu/8)(V^2/L^3)$, where *J* is the current density, ε_o is permittivity of free space, ε is dielectric constant of the organic semiconductor blend, μ is the charge carrier mobility, *L* is the thickness of the active layer and *V* is the voltage drop across the device. For the measurement of mobility in pure system, an *n*-type heavily doped Si wafer with a SiO_2 layer of 300 nm and a capacitance of 11 nF/cm^2 was used as the gate electrode and dielectric layer. Thin films of C-PCBSD and C-PCBSD with varying concentration of FPI dopant were deposited on SiO_2/Si

substrates by spin-coating their DCB solution. Gold source and drain contacts (40 nm in thickness) were deposited by vacuum evaporation on the organic layer through a shadow mask, affording a bottom-gate, top-contact organic thin film transistor (OFET) device. Electrical measurements of the OFET devices were carried out at room temperature in air using a 4156C Semiconductor Parameter Analyzers, Agilent Technologies. The field-effect mobility was calculated in the saturation regime by using the equation, $I_{ds} = (\mu WC_i/2L)(V_g - V_t)^2$, where I_{ds} is the drain-source current, μ is the field-effect mobility, W is the channel width (1 mm), L is the channel length (0.1 mm), C_i is the capacitance per unit area of the gate dielectric layer, V_g is the gate voltage and V_t is threshold voltage.

3. Results and Discussion

3.1 Solvent-resistant test

In the previous study, the crosslinked PCBSD fullerene network offers a robust and adhesive thin film to improve the contact between ZnO and active layer.[27] To study the solvent resistance of the C-PCBSD network with different FPI-doped concentration, we spin-coated the pure PCBSD, PCBSD with 25 wt% FPI, and PCBSD with 50 wt% FPI onto the glass substrate followed by thermal heating at 170 °C for 15 min for crosslinking. Because FPI can be dissolved by nonpolar (o-dichlorobenzene denoted ODCB) and polar (DMF, isopropanol denoted IPA) solvents used for the processing of an active layer, the absorption spectra of the thin films were monitored before and after washing with ortho-dichlorobenzene (ODCB), IPA and DMF sequentially. It was found that the absorption spectra of C-PCBSD film remains unchanged before and after solvent rinsing (**Figure 2a**), indicating good solvent-resistance of C-PCBSD network. The similar results can be seen in the C-PCBSD (FPI, 25%) and C-PCBSD (FPI, 50%) thin films (**Figure 2b** and **2c**). This result indicates that the cross-linked network of C-PCBSD can sufficiently protect the embedded FPI dopant from being dissolved by the solvent.

3.2 The mobility effect with different FPI dopant concentration in C-PCBSD thin film under SCLC and OFET measurement

Having demonstrated that the C-PCBSD (FPI, 25%) and C-PCBSD (FPI, 50%) have good solvent resistance to realize the solution-processed layer-by-layer device fabrication, we further investigated the concentration effect of the FPI dopant on the mobility of the C-PCBSD/FPI layer.[41] The electron mobility (μ_e) of C-PCBSD, C-PCBSD (FPI, 25 wt%), and C-PCBSD (FPI, 50 wt%) thin films were measured by the SCLC devices. The results are shown in **Figure 3** and summarized in **Table 1.** The undoped C-PCBSD exhibited a μ_e of 1.3×10^{-5} $cm^2V^{-1}s^{-1}$, indicating its moderate semiconductor property in nature. Upon incorporating 25 wt% FPI dopant, the mobility enhanced to 2.4×10^{-5} $cm^2V^{-1}s^{-1}$. Moreover, when the dopant concentration increased to 50 wt%, the μ_e was further increased to 6.0×10^{-5} $cm^2V^{-1}s^{-1}$. The SCLC electron-only devices ITO/ZnO/C-PCBSD with or without FPI/P3HT:PCBM/Ca/Al with the

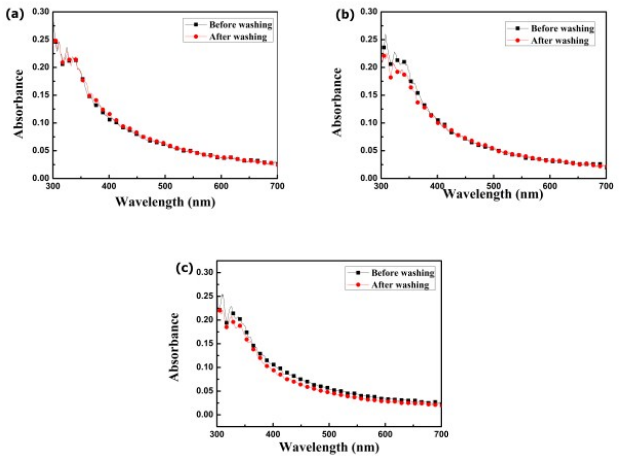

Figure 2. Thin film absorption spectra of (a) C-PCBSD (b) C-PCBSD (FPI, 25%) and (c) C-PCBSD (FPI, 50%) before and after washing by ODCB, IPA and DMF.

P3HT:PCBM active layer may not truly reveal the improved mobility of the PCBSD with FPI. To address this issue, we directly fabricated OFET devices using C-PCBSD as an n-type material with or without FPI. We found that the OFET mobility increases by two orders of magnitude from 3.8×10^{-6} $cm^2V^{-1}s^{-1}$ to 8.4×10^{-4} $cm^2V^{-1}s^{-1}$ when the doping concentration increased from 0 to 50%. The results are shown in **Figure S1** and summarized in **Table S1.** The undoped C-PCBSD exhibited an n-channel OFET characteristics with a μ_e of 3.8×10^{-6} cm^2 V^{-1} s^{-1}. Upon incorporating 25 wt% FPI dopant, the enhanced μ_e of 3.9×10^{-4} $cm^2V^{-1}s^{-1}$ by two orders of magnitude was obtained. Moreover, when the dopant concentration increased to 50 wt%, the μ_e was further increased to 8.4×10^{-4} $cm^2V^{-1}s^{-1}$. These results indicated that doping is effective for improving the electron mobility of C-PCBSD.

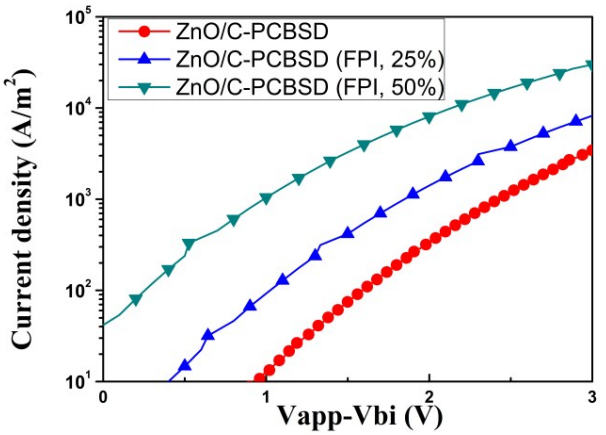

Figure 3. *J-V* characteristics of electron-only devices with different CBLs.

Table 3. Summary of SCLC device performance of C-PCBSD with varying FPI dopant concentration

Material	Electron mobility ($cm^2 V^{-1} s^{-1}$)
C-PCBSD	1.3×10^{-5}
C-PCBSD (FPI, 25%)	2.4×10^{-5}
C-PCBSD (FPI, 50%)	6.0×10^{-5}

3.3 Device performance of BHJPSCs, PHJPSCs, and measurement of external quantum efficiency (EQE)

The inverted BHJPSC using ZnO, ZnO/C-PCBSD, and ZnO/C-PCBSD (FPI, 50%) as the CBLs were first evaluated in the P3HT:$PC_{61}BM$ active layer system. ITO/ZnO(40 nm)/P3HT:$PC_{61}BM$ (1:1, w/w)(180 nm)/MoO_3 (7 nm)/Ag (150 nm) denoted as Device A**,** ITO/ZnO (40 nm)/C-PCBSD/P3HT:$PC_{61}BM$ (1:1, w/w) (180 nm)/MoO_3 (7 nm)/Ag (150 nm) denoted as Device B, and ITO/ZnO (40 nm)/C-PCBSD (FPI, 50%)/P3HT:$PC_{61}BM$ (1:1, w/w)(180 nm)/MoO_3 (7 nm)/Ag (150 nm) denoted as Device C were therefore we fabricated. The structures of devices and chemicals were shown in **Figure 4**. The *J – V* characteristics of Device A, B, and C are shown in **Figure 5** and summarized in **Table 2.** Device A delivered a PCE to 3.5% with a V_{oc} of 0.56 V, a J_{sc} of 9.1 mA/cm^2, and an *FF* of 53%. With C-PCBSD as the interlayer in Device B to suppress leakage current, a higher PCE of 3.6% was reached with a V_{oc} of 0.56 V, a J_{sc} of 9.7 mA/cm^2 and a *FF* of 67%. Finally, device C where C-PCBSD (FPI, 50%) was adopted as the interlayer delivered a higher PCE of 3.9% with a V_{oc} of 0.57 V, a J_{sc} of 10.1 mA/cm^2, and a *FF* of 67%. The improved performance with better current was attributed to the enhanced electron mobility through AIET.

Meanwhile, to further test its universal application, a low-band gap polymer PBDTTT-C-T (**Figure 4c)** blended with $PC_{71}BM$ was also employed to evaluate the photovoltaic performances ITO/ZnO (40 nm)/PBDTTT-C-T: $PC_{71}BM$ (1:1.5, w/w)/MoO_3 (7 nm)/Ag (150 nm) denoted as Device D. ITO/ZnO (40 nm)/C-PCBSD/PBDTTT-C-T: $PC_{71}BM$ (1:1.5, w/w)/MoO_3 (7 nm)/Ag (150 nm) denoted as Device E, and ITO/ZnO (40 nm)/C-PCBSD (FPI, 50%)/PBDTTT-C-T:$PC_{71}BM$ (1:1.5, w/w)/MoO_3 (7 nm)/Ag (150 nm) denoted as Device F were fabricated. The *J – V* characteristics of Device D, E, and F are shown in **Figure 6a** and summarized in **Table 2.** Device D delivered a PCE to 5.8% with a V_{oc} of 0.76 V, a J_{sc} of 13.1 mA/cm^2, and an *FF* of 58%. In a similar manner, a higher PCE of 6.0% was reached in Device E with a V_{oc} of 0.76 V, a J_{sc} of 13.8 mA/cm^2, and an *FF* of 57%. A superior PCE of 6.7% was achieved in Device F with a V_{oc} of 0.76 V, a J_{sc} of 15.4 mA/cm^2, and an *FF* of 56%. The presence of the C-PCBSD interlayer in Device E slightly enhanced the EQE spectra from 500 nm to 800 nm as shown in **Figure 6b** and delivered a higher J_{sc} of 13.28 mA/cm^2 than12.50 mA/cm^2 calculated from Device D. Furthermore, the current of Device F increased to 14.82 mA/cm^2 when 50 wt% FPI was doped into C-PCBSD interlayer. Again, the increase photocurrent can be attributed to the improved exciton dissociation and diminished series resistance via AIET process.

To further confirmed the role of FPI dopant in C-PCBSD thin film, the planar heterojunction device was fabricated for the purpose of precluding the influence of PCBM. These device architectures are ITO/ZnO (40 nm)/PBDTTT-C-T/MoO_3 (7 nm)/Ag (150 nm) as Device G, ITO/ZnO (40 nm)/C-PCBSD/ PBDTTT-C- T/MoO_3 (7 nm)/Ag (150 nm) denoted as Device H, and ITO/ZnO)(40 nm)/C-PCBSD (FPI, 50%)/PBDTTT-C-T/MoO_3 (7 nm)/Ag (150 nm) denoted as Device I. The *J – V* characteristics of Device G, H, and I are shown in **Figure 7.** and summarized in **Table 2.** Device G delivered a PCE to 0.1% with a V_{oc} of 0.88 V, a J_{sc} of 0.29 mA/cm^2, and a *FF* of 36%. A higher PCE of 0.4% was reached in Device H with a V_{oc} of 0.86 36%. A higher PCE of 0.4% was reached in Device H with a V_{oc} of 0.86 V, a J_{sc} of 1.19 mA/cm^2, and a *FF* of 37%. Once again, the presence of C-PCBSD diminished the series resistance and offer extra exciton dissociation with the enhancement of J_{sc}. More encouragingly, Device I delivered an outperforming PCE of 0.6% with a V_{oc} of 0.76 V, a J_{sc} of 2.28 mA/cm^2, and a *FF* of 34%. The C-PCBSD (FPI, 50%) with the enhanced of mobility via AIET can extract more electron carriers from polymers.

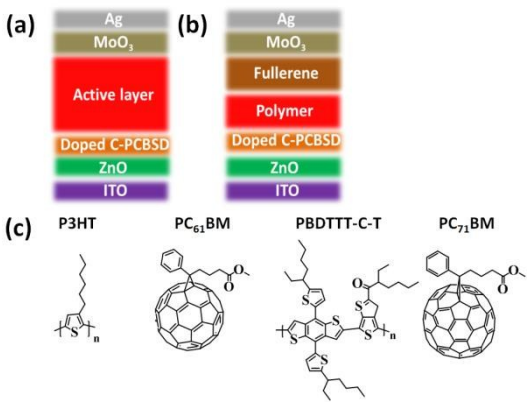

Figure 4. Schematic illustrations of the device architecture and compounds in (a) BHJPSCs; and (b) PHJPSCs. (c) Chemical structures of P3HT, $PC_{61}BM$, PBDTTT-C-T, and $PC_{71}BM$.

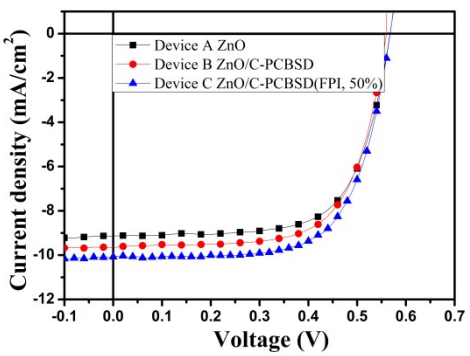

Figure 5. *J-V* characteristics of P3HT:$PC_{61}BM$ (1:1,w/w) in BHJPSCs with different CBLs.

Journal Name

RSCPublishing

Article

Table 2. Summary of device performance in BHJPSCs and PHJPSCs with varying CBL

Device	Cathodic Buffer layer	V_{oc} (V)	J_{sc} (mA/cm^2)	FF (%)	R_s (Ω-cm^2)	PCE (%)
A	ZnO	0.56	9.1	68	8.3	3.5
B	ZnO/C-PCBSD	0.56	9.7	67	6.2	3.6
C	ZnO/C-PCBSD (FPI, 50%)	0.57	10.1	67	5.5	3.9
D	ZnO	0.76	13.1 (12.5)[a]	58	7.3	5.8
E	ZnO/C-PCBSD	0.76	13.8 (13.3)[a]	57	7.2	6.0
F	ZnO/C-PCBSD (FPI, 50%)	0.76	15.4 (14.8)[a]	56	6.7	6.7
G	ZnO	0.88	0.3	36	202.0	0.1
H	ZnO/C-PCBSD	0.86	1.2	37	87.6	0.4
I	ZnO/C-PCBSD (FPI, 50%)	0.76	2.3	34	6.0	0.6

[a]Calculated from EQE.

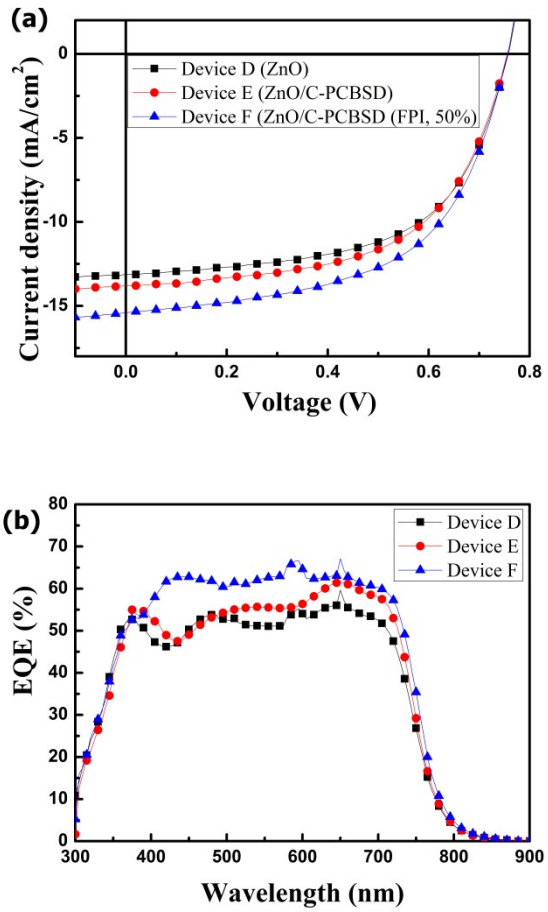

Figure 6. *J-V* characteristics of PBDTTT-C-T in PHJPSCs with different CBLs. (1:1.5,w/w) in BHJPSCs with different CBLs (b) The EQE spectrum of Device D, E, and F.

3.4 Device performance of OMPSCs and measurement of external quantum efficiency (EQE)

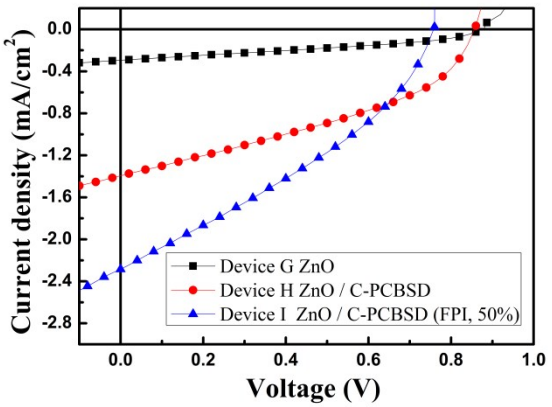

Figure 7. *J-V* characteristics of PBDTTT-C-T in PHJPSCs with different CBLs.

The C-PCBSD/FPI system with increasing mobilities indeed enhances the device performance in BHJPSCs and PHJPSCs. It is therefore envisaged that this strategy can be further applied to the OMPSC-based devices. Photovoltaic performances were investigated with the architecture of ITO/ZnO (40 nm)/ $CH_3NH_3PbI_3$ (376 nm)/ spiro-OMeTAD (253 nm)/Au (80 nm) denoted as Device J, ITO/ZnO (40 nm)/ C-PCBSD/ $CH_3NH_3PbI_3$ (376 nm)/spiro-OMeTAD (253 nm)/Au (80 nm) denoted as Device K, and ITO/ZnO (40 nm)/C-PCBSD (FPI, 50%)/$CH_3NH_3PbI_3$ (376 nm)/ spiro-OMeTAD (253 nm)/Au (80 nm) denoted as Device L. The *J –V* characteristics of Device J, K, and L are shown in **Figure 8a** and summarized in **Table 3.** Device J delivered a PCE to 7.0% with a V_{oc} of 0.92 V, a J_{sc} of 14.1 mA/cm^2, and an FF of 54%. This similar device performance coincides with a recent study by Lee and coworkers.[42] Better PCE of 10.2% was obtained in Device K with a V_{oc} of 0.90 V, a *Jsc* of 18.1 mA/cm^2, and an FF of 64% when a C-PCBSD interlayer was adopted. The higher PCE

Journal Name

RSCPublishing

Article

Table 3. Summary of device performance in BHJPSCs and PHJPSCs with varying CBL

Device	Cathodic Buffer layer	V_{oc} (V)	J_{sc} (mA/cm^2)	FF (%)	R_s (Ω-cm^2)	PCE (%)
J	ZnO	0.92	14.1 (13.5)[a]	54	12.6	7.0
K	ZnO/C-PCBSD	0.88	18.0 (16.4)[a]	64	7.7	10.2
L	ZnO/C-PCBSD (FPI, 50%)	0.90	19.1 (17.5)[a]	69	5.9	11.9

[a]Calculated from EQE.

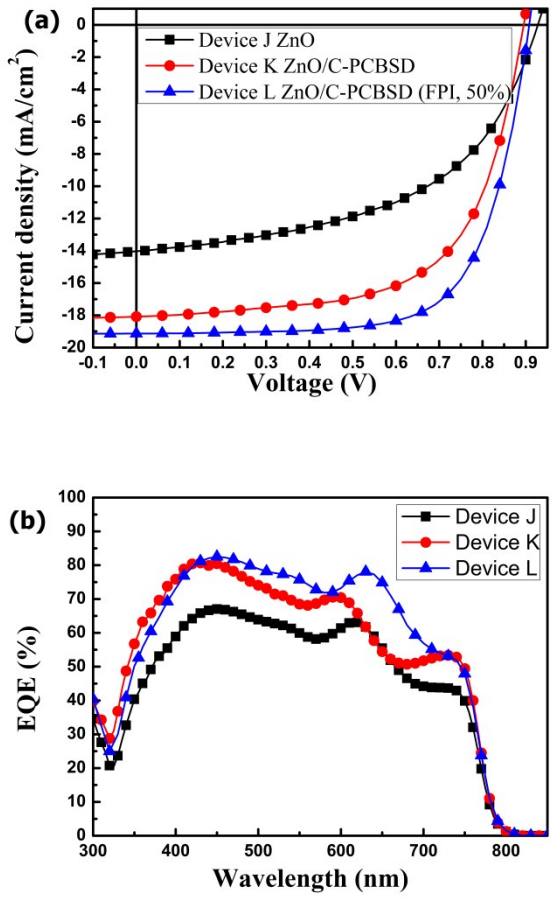

Figure 8. (a) *J-V* characteristics. of $CH_3NH_3PbI_3$ in OMPSCs with differe nt CBLs. (b) The EQE spectrum of Device J, K, and L.

resulted from the largely improved J_{sc}, and FF. Taking advantage of the improved mobility, Device L demonstrated animpressive PCE of 11.9% with a V_{oc} of 0.90 V, a J_{sc} of 19.1 mA/cm^2, and an FF of 69%. The result thus showed the potential use of FPI-doped C-PCBSD as a CBL in achieving better PCEs. Especially, as can be seen in **Figure 8b**, device K delivered enhanced EQE values from 350 to 750 nm as

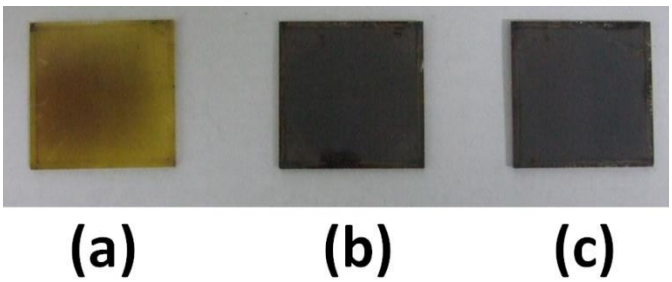

Figure 9. The thermal stability test (a) ITO/ZnO/$CH_3NH_3PbI_3$, 80^{o}C, 1 hour; (b) ITO/ZnO/C-PCBSD/$CH_3NH_3PbI_3$, 80^{o}C, 1 hour; (c) ITO/ZnO/C-PCBSD (FPI, 50%) /$CH_3NH_3PbI_3$, 80^{o}C, 1 hour.

compared to Device J. Moreover, when mobility of FPI:C-PCBSD were improved via AIET, device L exhibited much higher EQE values from 450 to 750 nm. According to a recent report, it was found that CBLs could affect the thermal stability of $CH_3NH_3PbI_3$. **Figure 9.** shows the images of $CH_3NH_3PbI_3$ films onto ZnO, C-PCBSD/ZnO, and C-PCBSD (FPI, 50%)/ZnO after annealing treatment at 80 ^{o}C for 1 hour. After 1 hour annealing, the $CH_3NH_3PbI_3$ film directly on ZnO changed color from dark brown to yellow. The yellow region indicated the formation of PbI_2 resulting from the decomposition of $CH_3NH_3PbI_3$. This result may imply that the residue moisture from ZnO diffuse into the active layer and degrade the perovskite layer. This result is consistent with a recent study by Gong and his coworkers.[26] Recently, Kelly and coworkers point out the degradation by acid-base interface between ZnO and $CH_3NH_3PbI_3$. The presense of C-PCBSD imply the more acidic surface than $CH_3NH_3PbI_3$ thin film. [43] In contrast, the color of the $CH_3NH_3PbI_3$ thin films deposited onto the C-PCBSD/ZnO or C-PCBSD (FPI, 50%)/ZnO layers remained unchanged during annealing treatment. This result demonstrated that the C-PCBSD/FPI system can function as a protecting layer to prevent the $CH_3NH_3PbI_3$ layer from moisture in OMPSCs.

4. Conclusion

In summary, we have developed a new fullerene-based CBL with enhanced mobility by incorporating an ionic FPI into the C-PCBSD network. By taking advantaging of high mobility of FPI dopant, the 50 wt% FPI-doped C-PCBSD interlayer can

substantially enhance the Jsc and PCE in PHJPSCs as well as OMPSCs. Meawhile, the C-PCBSD network can prevent the residue moisture from diffusing into perovksite layer, thus improving the thermal stability of the devices. Finally, this strategy offers a universal CBL to enhance the PCEs of BHJPSCs and OMPSC (5.8% to 6.7% and 7.0% to 11.9%, respectively) thourgh facilitating electron transfer between the active layer and an electrode.

Acknowledgements

This work was supported by the Ministry of Science and "ATP" project of the National Chiao Tung University and Ministry of
This work was supported by the Ministry of Science and "ATP" project of the National Chiao Tung University and Ministry of Education, Taiwan.

Notes and references

[a]Department of Applied Chemistry, National Chiao Tung University, 1001 Ta Hsueh Road Hsin-Chu, 30010 (Taiwan)
*E-mail: cshsu@mail.nctu.edu.tw
[b]Institute of Chemistry, Chinese Academy of Sciences, Bejing, 100190, China

1. M. H. Kumar, N. Yantara, S. Dharani, M. Graetzel, S. Mhaisalkar, P. P. Boix and N. Mathews, *Chem. Commun.*, 2013, **49**, 11089-11091.
2. M. Singh, H. M. Haverinen, P. Dhagat and G. E. Jabbour, *Adv. Mater.*, 2010, **22**, 673-685.
3. J. Seo, S. Park, Y. Chan Kim, N. J. Jeon, J. H. Noh, S. C. Yoon and S. I. Seok, *Energy Environ. Sci.*, 2014, **7**, 2642-2646.
4. Z. Xiao, C. Bi, Y. Shao, Q. Dong, Q. Wang, Y. Yuan, C. Wang, Y. Gao and J. Huang, *Energy Environ. Sci.*, 2014, **7**, 2619-2623.
5. S. Luo and W. A. Daoud, *J. Mater. Chem. A*, 2015. DOI: 10.1039/c1034ta04953e
6. P. V. Kamat, *J. Phy. Chem. Lett.*, 2013, **4**, 908-918.
7. J.-H. Im, I.-H. Jang, N. Pellet, M. Grätzel and N.-G. Park, *Nat. Nanotechnology*, 2014, **9**, 927-932.
8. P.-W. Liang, C.-C. Chueh, X.-K. Xin, F. Zuo, S. T. Williams, C.-Y. Liao and A. K. Y. Jen, *Adv. Energy Mater.*, 2015, **5**, 1400960-1400966
9. C.-W. Chen, H.-W. Kang, S.-Y. Hsiao, P.-F. Yang, K.-M. Chiang and H.-W. Lin, *Adv. Mater.*, 2014, **26**, 6647-6652.
10. D. Liu, M. K. Gangishetty and T. L. Kelly, *J. Mater. Chem. A*, 2014, **2**, 19873-19881.
11. C.-H. Chiang, Z.-L. Tseng and C.-G. Wu, *J. Mater. Chem. A*, 2014, **2**, 15897-15903.
12. Q. Xue, Z. Hu, J. Liu, J. Lin, C. Sun, Z. Chen, C. Duan, J. Wang, C. Liao, W. M. Lau, F. Huang, H.-L. Yip and Y. Cao, *J. Mater. Chem. A*, 2014, **2**, 19598-19603.
13. K.-C. Wang, P.-S. Shen, M.-H. Li, S. Chen, M.-W. Lin, P. Chen and T.-F. Guo, *ACS Appl. Mater. Interfaces*, 2014, **6**, 11851-11858.
14. J. Zhang, P. Barboux and T. Pauporté, *Adv. Energy Mater.*, 2014, **9**. 1400932-1400939.
15. A. Kojima, K. Teshima, Y. Shirai and T. Miyasaka, *J. Am. Chem. Soc.*, 2009, **131**, 6050-6051.
16. J.-H. Im, C.-R. Lee, J.-W. Lee, S.-W. Park and N.-G. Park, *Nanoscale*, 2011, **3**, 4088-4093.
17. M. M. Lee, J. Teuscher, T. Miyasaka, T. N. Murakami and H. J. Snaith, *Science*, 2012, **338**, 643-647.
18. H. Zhou, Q. Chen, G. Li, S. Luo, T.-b. Song, H.-S. Duan, Z. Hong, J. You, Y. Liu and Y. Yang, *Science*, 2014, **345**, 542-546.
19. S. N. Habisreutinger, T. Leijtens, G. E. Eperon, S. D. Stranks, R. J. Nicholas and H. J. Snaith, *Nano Lett.*, 2014, **14**, 5561-5568.
20. H.-S. Kim, C.-R. Lee, J.-H. Im, K.-B. Lee, T. Moehl, A. Marchioro, S.-J. Moon, R. Humphry-Baker, J.-H. Yum, J. E. Moser, M. Gratzel and N.-G. Park, Sci. Rep., 2012, 2, 591.
21. A. Mei, X. Li, L. Liu, Z. Ku, T. Liu, Y. Rong, M. Xu, M. Hu, J. Chen, Y. Yang, M. Grätzel and H. Han, *Science*, 2014, **345**, 295-298.
22. M. He, D. Zheng, M. Wang, C. Lin and Z. Lin, *J. Mater. Chem. A*, 2014, **2**, 5994-6003.
23. D. Liu and T. L. Kelly, *Nat. Photonics*, 2014, **8**, 133-138.
24. T. Leijtens, G. E. Eperon, S. Pathak, A. Abate, M. M. Lee and H. J. Snaith, *Nat. Commun.*, 2013, **4**.
25. I. Gonzalez-Valls and M. Lira-Cantu, *Energy Environ. Sci.*, 2009, **2**, 19-34.
26. Q. Hu, J. Wu, C. Jiang, T. Liu, X. Que, R. Zhu and Q. Gong, *ACS Nano*, 2014, **8**, 10161-10167.
27. C.-H. Hsieh, Y.-J. Cheng, P.-J. Li, C.-H. Chen, M. Dubosc, R.-M. Liang and C.-S. Hsu, *J. Am. Chem. Soc.*, 2010, **132**, 4887-4893.
28. A. Abrusci, S. D. Stranks, P. Docampo, H.-L. Yip, A. K. Y. Jen and H. J. Snaith, *Nano Lett.*, 2013, **13**, 3124-3128.
29. J.-Y. Jeng, Y.-F. Chiang, M.-H. Lee, S.-R. Peng, T.-F. Guo, P. Chen and T.-C. Wen, *Adv. Mater.*, 2013, **25**, 3727-3732.
30. Y. I. H. Chao, J.-F. Jheng, J.-S. Wu, K.-Y. Wu, H.-H. Peng, M.-C. Tsai, C.-L. Wang, Y.-N. Hsiao, C.-L. Wang, C.-Y. Lin and C.-S. Hsu, *Adv. Mater.*, 2014, **26**, 5205-5210.
31. Y.-J. Cheng, C.-H. Hsieh, P.-J. Li and C.-S. Hsu, *Adv. Funct. Mater.*, 2011, **21**, 1723-1732.
32. H.-L. Yip and A. K. Y. Jen, *Energy Environ. Sci.*, 2012, **5**, 5994-6011.
33. Y.-Y. Lai, Y.-J. Cheng and C.-S. Hsu, *Energy Environ. Sci.*, 2014, **7**, 1866-1883.
34. C.-Z. Li, C.-Y. Chang, Y. Zang, H.-X. Ju, C.-C. Chueh, P.-W. Liang, N. Cho, D. S. Ginger and A. K. Y. Jen, *Adv. Mater.*, 2014, **26**, 6262-6267.
35. N. Cho, C.-Z. Li, H.-L. Yip and A. K. Y. Jen, *Energy Environ. Sci.*, 2014, **7**, 638-643.
36. C.-Z. Li, C.-C. Chueh, F. Ding, H.-L. Yip, P.-W. Liang, X. Li and A. K. Y. Jen, *Adv. Mater.*, 2013, **25**, 4425-4430.
37. C.-Z. Li, C.-C. Chueh, H.-L. Yip, F. Ding, X. Li and A. K. Y. Jen, *Adv. Mater.*, 2013, **25**, 2457-2461.
38. C.-Z. Li, C.-C. Chueh, H.-L. Yip, K. O'Malley, W.-C. Chen and A. K. Y. Jen, *J. Mater. Chem.*, 2012, **22**, 8574-8578.
39. Y. Sun, J. H. Seo, C. J. Takacs, J. Seifter and A. J. Heeger, *Adv. Mater.*, 2011, **23**, 1679-1683.
40. L. Huo, S. Zhang, X. Guo, F. Xu, Y. Li and J. Hou, *Angew. Chem.*, 2011, **50**, 9697-9702.
41. M.-A. Muth, W. Mitchell, S. Tierney, T. Lada, X. Xue, H. Richter, M. Carrasco-Orozco and M. Thelakkat, *Nanotechnology* 2013, **24**, 484001-484009.
42. J. Kim, G. Kim, T. K. Kim, S. Kwon, H. Back, J. Lee, S. H. Lee, H. Kang and K. Lee, *J. Mater. Chem. A*, 2014, **2**, 17291-17296.

43. J. Yang, B. D. Siempelkamp, E. Mosconi, F. Angelis and T. L. Kelly, *Chem. Mater.*, 2015, **27**, 4229-4236.